Arabian Journal of Geosciences (2020) 13:1150
https://doi.org/10.1007/s12517-020-06109-9

ORIGINAL PAPER

# Time-dependent performance of damaged marble and corresponding fractional order creep constitutive model

Jing Chen[1] · Quan Jiang[2] · Yanran Hu[1] · Weimin Qin[2] · Shaojun Li[2] · Jun Xiong[3]

Received: 5 November 2019 / Accepted: 6 October 2020


**Abstract**
The time-dependent behaviour of a rock mass is crucial to the long-term stability of underground engineering projects, such as large tunnels, caverns and roadways. This paper focused on the experimental and theoretical studies of marble creep behaviour considering its initial damage due to excavation damage. Based on the onsite investigation of the creep performance of Jinping marble, detailed creep tests were carried out on damaged marble under different confining stresses, which indicated that damaged marble exhibited more notable creep properties than the intact marble. A new time-dependent creep constitutive model was proposed to characterize the time-dependent mechanical behaviour of damaged marble in terms of fractional derivatives and damage variables by replacing the Newtonian dashpot with the Abel dashpot. Furthermore, this one-dimensional creep equation was extended to a three-dimensional numerical model for analyzing the long-term deformation of hydraulic caverns. The simulation results indicated that the proposed model provided a precise description for the full creep process of marble containing initial damage.

**Keywords** Initial damage · Creep test · Fractional derivatives · Damage variables · Creep model

## Introduction

As Scheidegger (1970) stated, "The problem of the long-term behaviour of rocks is an important issue in connection with the construction of tunnels, dams and similar structures". The creep behaviour of the surrounding rock, as one of the important mechanical characteristics of rock over time, plays a key role in the stability of underground structures. In the early 1970s, it had been found that the hard and intact granite of a traffic tunnel in Switzerland had flaked 2 years after completion (Liu 2011). Due to the relatively weak quartzite and high geostress, many underground roadways in South African gold mines eventually experienced long-term deformation, which resulted in serious stability challenges (Malan 2002). Similarly, reinforcement was imposed on the surrounding rock of the Jinping I and Laxiwa hydropower stations due to the time-dependent deformation and breakage under high stress (Lu et al. 2010; Jiang et al. 2020a).

Many research works related to time-dependent deformation and failure have been carried out mainly from three aspects:

(1). The time-dependent behaviours of onsite rocks, e.g. Martino and Chandler (2004) conducted studies at the Underground Research Laboratory (URL), Canada; Feng et al. (2018a) observed the evolution of excavation-damaged zones and fractures of the internal displacement of hard surrounding rock masses; J. Herrmann et al. (2019) conducted constant stress deformation experiments at elevated confining pressures, $p(c)$ = 50–115 MPa, and temperatures, $T$ = 75–150 °C; and Jiang et al. (2019) exposed the time-dependent development of surface break performance and the inner cracking evolution of rock mass.

Responsible Editor: Zeynal Abiddin Erguler

✉ Quan Jiang
qjiang@whrsm.ac.cn

[1] School of Architectural Engineering, Tongling University, Tongling 244061, Anhui, People's Republic of China

[2] State Key Laboratory of Geomechanics and Geotechnical Engineering, Institute of Rock and Soil Mechanics, Chinese Academy of Sciences, Wuhan 430071, China

[3] Department of Civil and Environmental Engineering, University of Alberta, Edmonton T6G 2W2, Canada

Published online: 28 October 2020

(2). Laboratory creep experiments, e.g. Xu et al. (2012) analysed the variations in seepage rate with time in complete creep processes of rock due to the growth of creep cracks; Rassouli and Zoback (2017) found that shale samples experienced the same creep trend overtime, regardless of the loading history; Paraskevopoulou et al. (2018) tested low Jurassic and Cobourg limestone samples at different static load levels in unconfined conditions; Zhao et al. (2019) conducted six brittle creep and two ductile creep experiments on Jinping marble under true triaxial stress conditions; Shi et al. (2019) carried out acoustic emission (AE) experiments to study short-time creep behaviour under uniaxial compression for cuboid-shaped fine sandstone specimens with two pre-existing cracks; and Yang et al. (2019) performed uniaxial compressive creep experiments of medium-coarse sandstone from the columns of the Yungang Grottoes on both dried and water-saturated samples.

(3). Creep constitutive models, e.g. Feng et al. (2004) proposed a new system identification method for the simultaneous establishment of a viscoelastic rock material model structure; Weng (2014) proposed a constitutive model to describe the time-dependent behaviour and wetting deterioration of sandstone; Yang et al. (2015) recommended a new nonlinear viscoelastic and accelerating creep model to describe the complete creep curve of coal; Vakili (2016) presented the theoretical backgrounds, guidelines for selection of inputs, validation, and limitations/assumptions for a proposed improved unified constitutive model (IUCM); Bian et al. (2019) established a damage constitutive model of rock subjected to water-weakening effect and uniaxial loading by considering the influence of void-compression stage; and Wang et al. (2020) proposed a new creep damage constitutive model to describe the creep property of salt rock under uniaxial compression.

Although these outstanding endeavours have notably increased the understanding of the time-dependent behaviour of rock material, many studies on rock creep have focused on intact rock but have ignored damaged rock (Wang et al. 2018; Zhang et al. 2015). It is well known that the mechanical properties of rock will deteriorate in the process of blasting excavation and complex loading-unloading disturbances in underground engineering (Brady and Brown 1985; Millard et al. 2009; Sharifzadeh et al. 2010; Cai et al. 2018; Jiang et al. 2020b), which often results in a time-dependent instability risk due to the surrounding rock failure. Thus, a suitable time-dependent constitutive model considering the initial damage of rock remains a challenging problem.

Fractional calculus, as a powerful tool for modelling viscoelastic and viscoplastic behaviours, has been applied to develop creep constitutive models. In the early stage, the contributions of Rogers (1983), Bagley and Torvik (1983) and Koeller (1984, 2007) were remarkable, and the theory of fractional calculus has also been widely used on different kinds of materials in the past few decades. Zhou et al. (2011) proposed a creep constitutive model for salt rock by replacing the Newtonian dashpot in the classical Nishihara model with the fractional derivative Abel dashpot. Kawada et al. (2013) proposed the orders of fractional derivative for viscoelastic behaviours of rocks and minerals. Wu et al. (2015) presented a new method for building creep models for rock based on variable-order fractional derivatives. Xu and Jiang (2017) employed three sets of creep experimental data for polymer and rock e to demonstrate the effectiveness of fractional derivative models. Hu et al. (2018) presented a nonlinear elastic-viscoplastic rheological model characterize the time-based deformational behaviour of hard rock. These prominent works indicated that the fractional calculus theory has a certain advantage in describing the rock rheologic. Pu et al. (2020) established a fractional order viscoelastoplastic constitutive model to describe the creep characteristics of rock under cyclic loading and reflect the presented fluctuation of strain curve of rock under cyclic loading. Liu et al. (2020) presented a nonlinear fractional damage creep model by combining the improved viscoelastic model and proposed damage model to describe the creep mechanical behaviour of sandstone.

In this paper, onsite investigation and creep tests were carried out firstly to acquire the time-dependent mechanical behaviours of damaged marble in underground caverns. Then, a new one-dimensional creep constitutive model is proposed for marble with initial damage based on fractional derivatives and damage variables. Moreover, the three-dimensional creep constitutive model was extended to analyse the long-time deformation performance of a hydraulic underground cavern.

## Onsite investigation of Jinping marble

### Background of the Jinping II hydropower station

The Jinping II hydropower station, with a total installed capacity of 4800 MW in Sichuan Province, China, is mainly composed of barrages, diversion tunnels and underground caverns. It is the largest underground hydraulic engineering project in the Yalong River region, with the main powerhouse and main transformer room being 352.4 m × 28.5 m × 72.1 m and 374.6 m × 19.8 m × 35.1 m (length × width × height), respectively, in size. The measured maximum principal stress is 17 to 23 MPa, with a trend normal to the Yalong River. The rock stratum is a Triassic marble, i.e. $T_{2y}$ and $T_{2z}$. Its uniaxial compressive strength (UCS) ranges from 70 to 90 MPa. To study the mechanical creep properties of Jinping marble, we gathered marble samples during the excavation of the underground powerhouse.

### Time-dependent phenomenon by field investigation

The in-site time-dependent deformation and failure phenomenon were observed in Jinping II hydropower station caverns (Li et al. 2011; Feng et al. 2018b); after the underground caverns of the Jinping II hydropower station were excavated, the long-term stability of caverns during operation period would be still notable. The time-dependent failure of the surrounding rock and supporting structure had been investigated 3 years after excavation. Since the excavation of the Jinping II underground caverns was completed on 30 June 2010, we conducted the in situ investigation in August 2013, and the start time of the long-term monitoring data was also set in July 2010.

The main powerhouse had been designed for electricity generation in 2010. However, there were many small auxiliary tunnels around the main powerhouse and the main transformer room, such as drainage tunnels and abandoned construction tunnels, which provided us the chance to study the time-dependent performance of the onsite marble. In these tunnels, certain typical time-dependent failure behaviour had been observed, including the shallow cracking of the marble surrounding the tunnel, spalling and breakage of the shotcrete on the tunnel's surface and localized marble detachment in the tunnel, as shown in Fig. 1.

The in situ investigations indicated that the marble in the excavation damage zone exhibited time-dependent behaviours obviously. Thus, detailed experimental and theoretical analyses of the creep characteristics were necessary for the Jinping II marble with initial damage.

## Creep experimental study of damaged marble

### Preparation of the initial damaged marble sample

To reduce the material differences and ensure the initial damage in different specimens was approximate, we selected the specimens by three ways:

(i). All specimens were obtained at the same location in the Jinping II underground powerhouse.
(ii). Before making initial damage marbles, we kicked off some which had fissures, breakage or impurity; then, acoustic test was conducted to pick out specimens which had similar wave velocities.
(iii). After initial damage marbles were made, acoustic test was put to use once again to choose specimens had similar wave velocities.

Martin (1993) proposed that the stable growth of micro-cracks inside rock occurred when the compressive stress loaded on the specimen was 40–80% of its instant peak strength. Based on this damage principle of hard rock, a compressive stress of nearly 80% of the marble's peak strength was imposed on cylindrical samples with heights of 100 mm and diameters of 50 mm, and this stress was maintained for half an hour under uniaxial compression conditions. As a result, marbles specimens with initial damage were gained.

In general, the more micro-cracks there are in the rock, the lower the velocity and the greater the attenuation are. Thus, acoustic testing and computed tomography (CT) scanning were applied to the marble specimens before and after preloading. These tests showed that the wave velocity of the damaged marble had a significant reduction after preloading with drops of 5.3%, 10.14%, 6.17%, 8.41%, 9.27% and 6.22% (Fig. 2a). After preloading, micro-damage was detected in these specimens (Fig. 2b). All these tests indicated that the preloading treatment resulted in comparable damage to the marble specimens.

### Scheme of the creep experiment

We consider the buried depth of the Jinping II hydropower station underground powerhouse and ground stress field test results, as well as the results of conventional triaxial compression tests with axial stresses 110 MPa, 125 MPa, 140 Mpa and 160 MPa under confining pressures of 5 MPa, 10 MPa, 20 MPa and 40 MPa, respectively. Then, triaxial creep tests


**Fig. 1** Typical time-dependent failures of Jinping marble

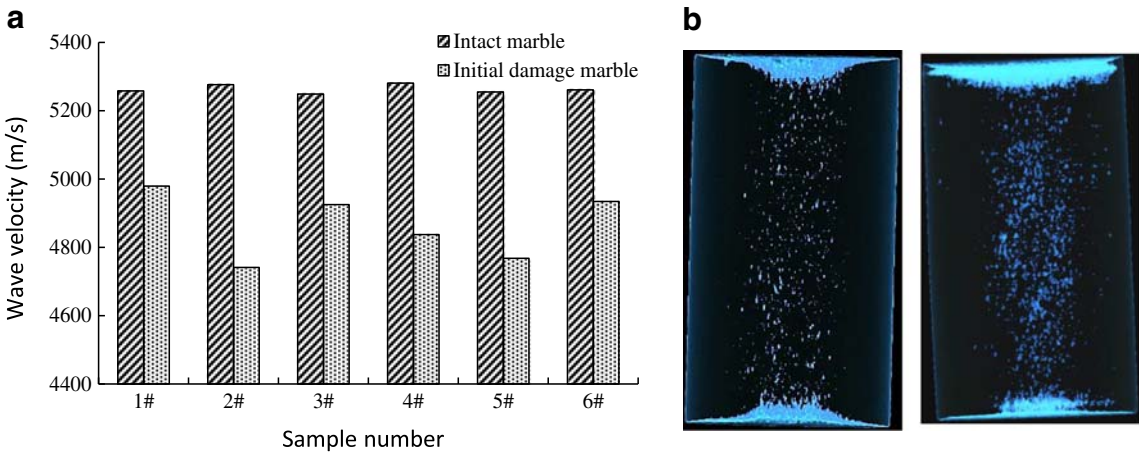


**Fig. 2** Comparison analysis of the intact and damaged marble specimens (**a** comparison of the marble specimen wave velocities before and after the preloading treatment; **b** micro-damage inside the marble specimens after preloading observed via CT scanning)

with these surrounding pressures were performed on initial damaged marble. The scheme details are summarized in Table 1. Here, the stress for initial damaged marble was also designed according to the conventional compressive testing results.

The tests were carried out on a servo-controlled triaxial rheological testing machine. On the basis of a traditional rheometer, a temperature-controlled triaxial chamber system is added to avoid any room temperature variation effects on the test results. During the creep tests, the axial deformation is measured by two LVDTs, and the lateral strain is measured by a ring sensor. The testing machine can apply a maximum axial stress of 200 MPa, and the confining pressure can reach up to 60 MPa. The creep tests were conducted using the following steps, while data were recorded by the sensors during the experimental process.

(i). The specimen wrapped with heat shrink tubing was placed in the pressure chamber and axial and lateral displacement sensors were then installed on the rock sample.

(ii). The confining pressure was applied at a rate of 1 MPa/min until the sample attained the set confining pressure after the indoor temperature was set to a range of 25 ± 0.5 °C.

(iii). The axial load was applied stepwise, and the first applied load step was 0.7 times the triaxial compressive strength of the specimen. A loading rate of 2 MPa/min was used at the loading stage. The axial stress was kept constant after the load reached the pre-set value.

(iv). The next axial stress step was applied based on whether the lateral deformational increment of the specimen was less than $1 \times 10^{-3}$ mm within 72 h.

(v). Each loading step of the axial stress was imposed with an increment of 10 MPa according to the above loading scheme until the rock failed (Table 1), at which point the test ended.

## Result analysis of the marble's creep tests

According to the above experimental scheme, the strain curves of the marble under different confining pressures were obtained, as shown in Fig. 3, where $\varepsilon_1$ is the axial strain, and $\varepsilon_2$ is the lateral strain. Based on these creep tests, certain typical time-dependent characteristics of damaged marble were elucidated.

Under lower deviatoric stress and lower confining pressure conditions (i.e. 5 MPa confining pressure and 70 MPa deviatoric stress), instantaneous deformation quickly occurred after the loading stress was applied, and the axial creep strain of the specimen under this loading stress quickly stabilized, which meant that the creep rate of the specimen decreased to 0 and only the attenuation creep stage occurred.

**Table 1** Test schemes of the creep tests for the initial damaged marble

| Specimen no. | Confining pressure ($\sigma_3$) (MPa) | Stress loading values ($\sigma_1$) (MPa) | | | | | | | |
|---|---|---|---|---|---|---|---|---|---|
| #1 | 5 | 70 | 80 | 90 | 100 | 110 | 120 | 130 | … |
| #12 | 10 | 80 | 90 | 100 | 110 | 120 | 130 | 140 | … |
| #13 | 20 | 90 | 100 | 110 | 120 | 130 | 140 | 150 | … |
| #15 | 40 | 100 | 110 | 120 | 130 | 140 | 150 | 160 | … |

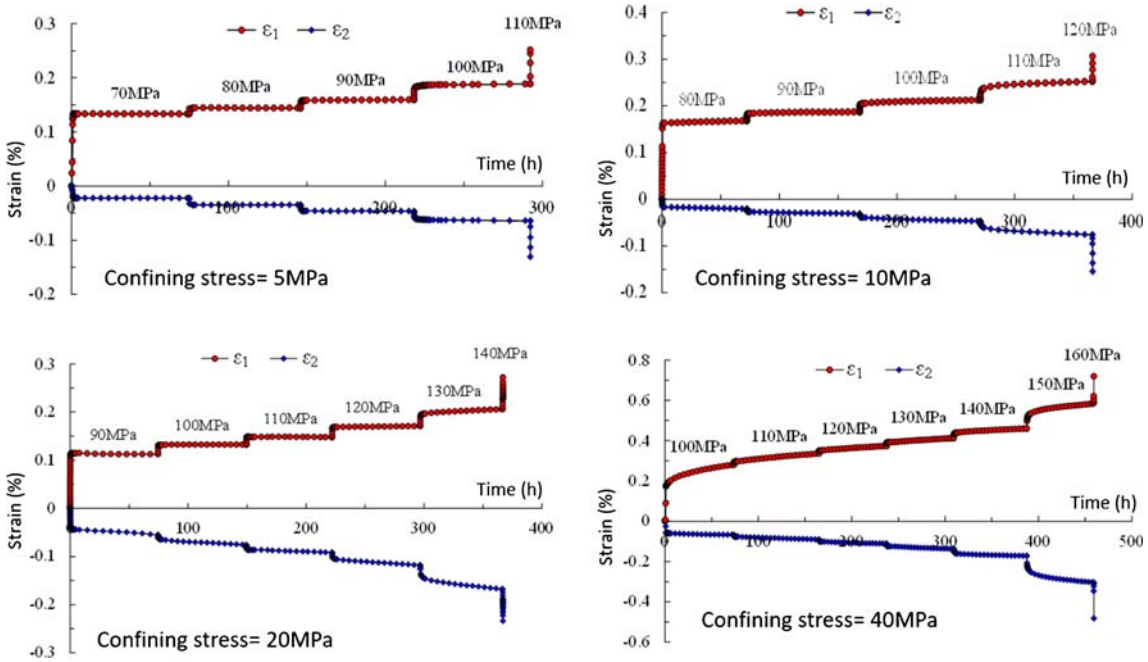


**Fig. 3** Typical creep strain curves over time of the initial damaged marble under different confining pressures

When the axial load was nearly 80% of the triaxial strength of the specimen and the confining pressure was relatively high, the creep rate of the specimen tended to remain stable (i.e. 10 MPa confining pressure and 100 MPa deviatoric stress), which indicated the steady creep stage generated. This macro-scale performance indicated that micro-cracks were initiated and damage creep began to occur at this loading level. However, this loading level was not high enough to cause accelerated crack extension and further damage inside the specimen.

When the constant load was nearly equal to the specimen's triaxial strength, the creep rate increased rapidly until the rock failed. This damage process was so short that accelerated creep and failure occurred very suddenly in general.

Furthermore, we found that the higher the confining pressure was, the earlier the steady creep stage appeared at a lower stress intensity ratio, i.e. the steady creep stage appeared when the stress intensity ratio was 0.83 under 10 MPa confining pressure, while the steady creep stage appeared when the stress intensity ratio was 0.69 under 40 MPa confining pressure.

What's more, triaxial creep tests with surrounding pressures of 5 MPa, 10 MPa, 20 MPa and 40 MPa were performed on undamaged marble, creep strain curves over time were given and the creep property comparison between initial damage marble and undamaged marble was illustrated (Chen 2013).

## Break characteristics of the specimens after the creep tests

After test, the macro-scale break patterns of the creep marbles were presented. These marble specimens exhibited single-shear failure under lower confining pressures (i.e.5 MPa and 10 MPa), and exiguous rock fragments can be observed on the main rupture surface. However, the initial damaged marble presented ductile failure with distinct volume increases under high axial stress and high confining pressures, where the middle of the sample deflected outward, as well as exhibiting a drum shape. Figure 4 shows the micro-morphology photos of the broken marble observed by the CT scanner under the 40 MPa confining pressure. These results indicated that the initial damaged marble had a distinct shear zone with a large number of surrounding micro-cracks. The micro-cracks

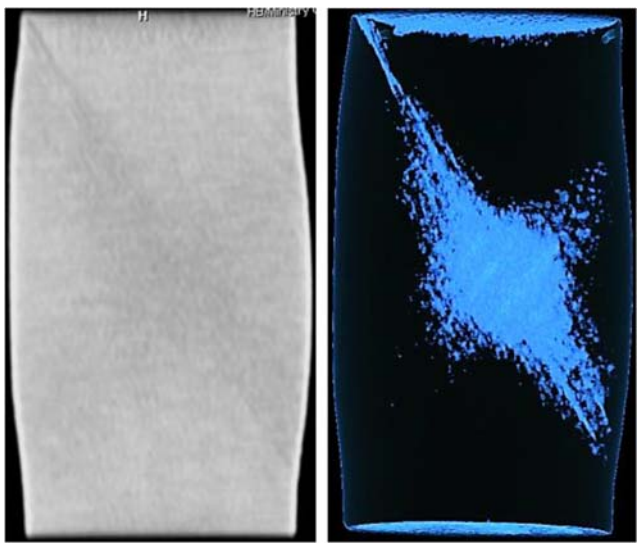

**Fig. 4** Micro-morphology CT photos of broken marble after creep test under 40 MPa confining pressure

accumulated in the centre and gradually developed towards both ends along the shear zone. This result declared that the cracks started to spread perpendicular to the shear zone, expanded into a drum shape and eventually resulted in shearing destruction.

## The fractional order time-dependent creep constitutive model

### The definition of the damage variables

Our experimental tests, including other engineering practices, have demonstrated that the long-term damage of rock is closely related to time-dependent. Studies on fractional calculus consider the time-dependent by many other researchers (Kawada et al. 2013, Zhou et al. 2016, Radmanesh and Ebadi 2020, Lu et al. 2020). In general, the total damage can be divided into two parts:

$$D(\sigma,t) = D\left(\sigma/\sigma_f\right) + D(t/t_F) \tag{1}$$

where $D(\sigma, t)$ is the total damage, $D(\sigma/\sigma_f)$ is the instantaneous damage caused by the stress variation and $D(t/t_F)$ is the time-dependent creep damage.

The increase in the instantaneous elastic deformation caused by the stress can be directly reflected to the variation of the instantaneous elastic modulus; therefore, the instantaneous elastic modulus changes can be defined as the instantaneous damage caused by the stress. Since the confining pressure under the given initial stress is not the same, the strength-stress ratio is used to describe the instantaneous damage variables.

$$D\left(\sigma/\sigma_f\right) = 1-E\left(\sigma/\sigma_f\right)/E_0 \tag{2}$$

where $\sigma$ is the current stress, $\sigma_f$ is the peak stress, whereby the regression relationship between the peak strength and confining pressure can be described as Eq. 3. $E_0$ is the instantaneous elastic modulus under the initial stress, and $E(\sigma/\sigma_f)$ is the instantaneous elastic modulus after stress loading. Considering that the instantaneous elastic deformation is independent of time, the instantaneous damage variable is only a function of the stress intensity ratio. The variations in the instantaneous elastic modulus and instantaneous damage variables with the stress under different confining pressures and axial loads are summarized in Table 2.

$$\sigma_f = 1.648\sigma_3 + 105.04 \tag{3}$$

The relationship between $D(\sigma/\sigma_f)$ and $\sigma/\sigma_f$ was shown in Eq. 4 which could be used to describe the instantaneous damage process of the marble containing initial damage.

$$D\left(\sigma/\sigma_f\right) = 1-\left(0.64 + 36.37\exp\left(-7.143\sigma/\sigma_f\right)\right) \tag{4}$$

Rock creep is a long time-dependent process, and creep damage is mainly caused by the rock deformation with loading time. Thus, based on the Norton power law equation proposed by Rabotnov (1963), the evolution equation with respect to the development of creep damage is obtained, assuming that the rock creep damage rate is as follows:

$$\frac{dD}{dt} = C\left(\frac{\sigma}{1-D}\right)^V \tag{5}$$

where $C$ and $V$ are rock material parameters, and the integration equation is given by the following:

$$-\frac{(1-D)^{V+1}}{v+1} = C\sigma^V t + C_1 \tag{6}$$

where $C_1$ is an integration constant.

If we assumed that there was no damage during the instantaneous loading, the initial conditions were $t = 0$ and $D = 0$. When the rock failed during the creep test, the structure of the specimen had been completely damaged, which meant $D = 1$. Therefore, $C_1$ can be calculated as follows:

$$C_1 = -\frac{1}{V+1} \tag{7}$$

Combining Eqs. 6 and 7, we can obtain Eq. 8.

$$D = 1-\left(1-C(V+1)\sigma^V t\right)^{\frac{1}{V+1}} \tag{8}$$

When $D = 1$, the rock creep failure time can be calculated as follows:

$$t_F = \left[C(V+1)\sigma^V\right]^{-1} \tag{9}$$

Equation 9 shows that $t_F$ has a negative exponential relation with the stress level. The higher the stress is, the shorter the creep life will be. The conclusion agrees with the experimental results of the initial damaged marble.

The relationship among the time-dependent damage variable, creep life and time are shown in Eq. 10 and can be deduced from Eqs. 8 and 9.

$$D(t/t_F) = 1-\left(1-\frac{t}{t_F}\right)^{\gamma} \tag{10}$$

where $\gamma = \frac{1}{V+1}$.

The smaller $\gamma$ is, the higher the creep acceleration rate is, which would result in further brittle failure. Conversely, brittle failure is characterized by ductile fractures.

**Table 2** Variations in the instantaneous elastic modulus and instantaneous damage variables with the stress

| Axial load (MPa) | Confining pressure (MPa) | | | | | | | | | | | |
|---|---|---|---|---|---|---|---|---|---|---|---|---|
| | 5 | | | 10 | | | 20 | | | 40 | | |
| | $\sigma/\sigma_f$ | $E(\sigma/\sigma_f)$ | $D(\sigma/\sigma_f)$ | $\sigma/\sigma_f$ | $E(\sigma/\sigma_f)$ | $D(\sigma/\sigma_f)$ | $\sigma/\sigma_f$ | $E(\sigma/\sigma_f)$ | $D(\sigma/\sigma_f)$ | $\sigma/\sigma_f$ | $E(\sigma/\sigma_f)$ | $D(\sigma/\sigma_f)$ |
| 70 | 0.6364 | 61.51 | 0 | | | | | | | | | |
| 80 | 0.7273 | 50.05 | 0.1863 | 0.6667 | 66.97 | 0 | | | | | | |
| 90 | 0.8182 | 47.84 | 0.2222 | 0.75 | 52.51 | 0.2159 | 0.6429 | 72.68 | 0 | | | |
| 100 | 0.9091 | 45.1 | 0.2668 | 0.8333 | 49.59 | 0.2595 | 0.7143 | 60.36 | 0.1695 | 0.625 | 75.49 | 0 |
| 110 | | | | 0.9167 | 47.32 | 0.2934 | 0.7857 | 55.99 | 0.2296 | 0.6875 | 62.96 | 0.166 |
| 120 | | | | | | | 0.8571 | 51.32 | 0.2939 | 0.75 | 58.58 | 0.224 |
| 130 | | | | | | | 0.9286 | 48.68 | 0.3302 | 0.8125 | 52.28 | 0.3075 |
| 140 | | | | | | | | | | 0.875 | 49.02 | 0.3506 |
| 150 | | | | | | | | | | 0.9375 | 47.18 | 0.375 |

## Time-dependent damage constitutive model based on the fractional order calculus theory

The fractional order calculus constitutive relation only requires a few parameters to establish the constitutive equation, which can describe the time effect well. Based on the fractional calculus theory and damage mechanics theory, a new time-dependent creep constitutive model was established to describe the creep mechanical behaviour evolution process of the original damaged marble.

### Riemann-Liouville fractional order calculus theory

The Riemann-Liouville fractional order calculus theory used widely is proposed in this study, and the fractional integral of order $\beta$ of function $f(t)$ is defined as follows:

$$\frac{d^{-\beta}f(t)}{dt^{-\beta}} = {}_{t_0}D_t^{-\beta}f(t) = \int_{t_0}^{t}\frac{(t-\tau)^{\beta-1}}{\Gamma(\beta)}f(\tau)d\tau \tag{11}$$

The fractional order calculus model is defined by the following:

$$\frac{d^{-\beta}f(t)}{dt^{\beta}} = {}_{t_0}D_t^{\beta}f(t) = \frac{d^n}{dt^n}\left[{}_{t_0}D_t^{-(n-\beta)}f(t)\right] \tag{12}$$

where $D^{-\beta}$ and $D^{\beta}$ are the Riemann-Liouville fractional integral operator and fractional derivative operator, respectively, with $\beta>0$ and $n-1<\beta\le n$, $n$ is a positive integer, $\Gamma(\beta)$ is the Gamma function, $\Gamma(\beta)=\int_0^{\infty}e^{-t}t^{\beta-1}dt$, $\mathrm{Re}(\beta)>0$ and $\mathrm{Re}(\beta)$ is the real part of $\beta$. The Laplace transform equation of the fractional order calculus model is the following:

$$L\left[{}_0D_t^{-\beta}f(t),p\right] = p^{-\beta}\overline{f}(p) \tag{13}$$

$$L\left[{}_0D_t^{\beta}f(t),p\right] = p^{\beta}\overline{f}(p) \tag{14}$$

If $f(t)$ approaches $t=0$, the function can be integrated.

### The constitutive equation of the Abel dashpot

The stress-strain relationship of an ideal solid should satisfy Hooke's law, as $\sigma(t)-\varepsilon(t)$, and the tress-strain relationship of an ideal fluid should satisfy Newton's viscosity law, as $\sigma(t)-d^1\varepsilon(t)/dt^1$. If we change $\sigma(t)-\varepsilon(t)$ to $\sigma(t)-d^0\varepsilon(t)/dt^0$, the Abel dashpot component can be defined as the soft component between the ideal solid and ideal fluid by replacing the Newtonian dashpot with the Abel dashpot.

Then, the constitutive equation of the Abel dashpot is the following:

$$\sigma(t) = \xi d^{\beta}\varepsilon(t)/\left(dt^{\beta}\right) \tag{15}$$

where $0\le\beta\le1$, and when $\beta=0$, the component is equal to the spring body, but when $\beta=1$, the component is equal to the Newton body; $\xi$ is a parameter similar to the elastic modulus of Hooke's law with the dimensional parameter $[\sigma\cdot t^{\beta}]$. The Abel dashpot, containing two components $\xi$ and $\beta$, not only can control the deformation rate but also can control the stress (strain). Thus, the Abel dashpot can describe the nonlinear creep process of the marble better. When $\sigma(t)$ = constant, the creep equation in Eq. 16 can be obtained from Eq. 15 with the fractional integral and a Laplace transform:

$$\varepsilon(t) = \frac{\sigma}{\xi}\frac{t^{\beta}}{\Gamma(1+\beta)},\quad 0\le\beta\le1 \tag{16}$$

where $\sigma$ is the initial constant stress. For different materials, the equation can be adjusted by the soft component

parameters (i.e. $\beta$ and $\xi$) to change the creep curve to fit the test results more adequately.

Because $0 \le \beta \le 1$, for$1 \le 1+\beta \le 2$ and $0 \le 1-\beta \le 1$, and thus the range of the independent variables $\Gamma(z)$ in the soft components ranges from 0 to 2. When $z=0$ and $\Gamma(z)$ are extremely large, the minimum value of $z$ is limited to 0.01. The fitting function is the following:

$$\Gamma(z) = \begin{cases} 0.909z^{-1.02} & (0.01 \le z \le 1) \\ 0.447z^2 - 1.326z + 1.869 & (1 < z \le 2) \end{cases} \quad (17)$$

## One-dimensional creep equation

For the purpose of describing the marble creep process precisely, a new improved fractional order time-dependent damage model was further put forward based on the above deduction, which was composed of the Hooke body, the Abel body, the Kelvin body and the Saint-Venant body, as shown in Fig. 5. In this model, the Kelvin body consists of a Hooke body parallel to a Newton body, and the Hooke body is used to show the instantaneous elastic properties, while the Abel body is used for describing the viscosity characteristics; the Kelvin body is constructed to describe the viscoelastic properties, and the Saint-Venant body is utilized to describe the plastic stage. When $\sigma < \sigma_f$, damage does worsen with time, and the model can represent decay creep and steady creep. When $\sigma \ge \sigma_f$, damage begins to increase with slip, the plastic component starts to exert an impact and the strength of the material decreases with time until the material fails.

In the figure above, $\varepsilon$ is the total stain; $\varepsilon_H$, $\varepsilon_A$ and $\varepsilon_K$ are the Hooke body strain, the Abel body strain and the Kelvin body strain, respectively; $\varepsilon_{VP}$ is the plastic component strain; $\varepsilon_M$ is composed of $\varepsilon_H$ and $\varepsilon_A$. Thus, the total strain can be written as follows:

$$\varepsilon = \varepsilon_M + \varepsilon_K + \varepsilon_{VP} \quad (18)$$

The stress-strain relationship of the Hooke body is as follows:

$$\varepsilon_H = \frac{\sigma}{E_0} \quad (19)$$

The stress-strain relationship of the Abel body is as follows:

$$\sigma = \xi \frac{d^\beta \varepsilon_A}{dt^\beta}, 0 \le \beta \le 1 \quad (20)$$

where $\xi$ is the viscosity coefficient of the Abel body.

The stress-strain relationship of the Kelvin body is:

$$\sigma = E_1 \varepsilon_K + \eta \dot{\varepsilon}_K \quad (21)$$

After integration, Eq. 21 can be rewritten as follows:

$$\varepsilon_K = \frac{\sigma}{E_1}\left[1 - \exp\left(-\frac{E_1}{\eta}t\right)\right] \quad (22)$$

Combining Eqs. 16, 19 and 22, the one-dimensional creep equation of the total strain can be described as Eq. 23.

$$\varepsilon = \frac{\sigma}{E_0} + \frac{\sigma}{\xi}\frac{t^\beta}{\Gamma(1+\beta)} + \frac{\sigma}{E_1}\left[1 - \exp\left(-\frac{E_1}{\eta}t\right)\right] \quad (23)$$

Substituting the damage variable into Eq. 23, the one-dimensional creep equation can be rewritten as follows:

$$\begin{cases} \varepsilon = \dfrac{\sigma}{E_0\left[1-D\left(\sigma/\sigma_f\right)\right]} + \dfrac{\sigma}{\xi[1-D(t/t_F)]}\dfrac{t^\beta}{\Gamma(1+\beta)} + \dfrac{\sigma}{E_1[1-D(t/t_F)]}\left[1-\exp\left(-\dfrac{E_1}{\eta}t\right)\right] & (\sigma < \sigma_f) \\ \varepsilon = \dfrac{\sigma}{E_0\left[1-D\left(\sigma/\sigma_f\right)\right]} + \dfrac{\sigma}{\xi[1-D(t/t_F)]}\dfrac{t^\beta}{\Gamma(1+\beta)} + \dfrac{\sigma}{E_1[1-D(t/t_F)]}\left[1-\exp\left(-\dfrac{E_1}{\eta}t\right)\right] + \varepsilon_{vp} & (\sigma \ge \sigma_f) \end{cases} \quad (24)$$

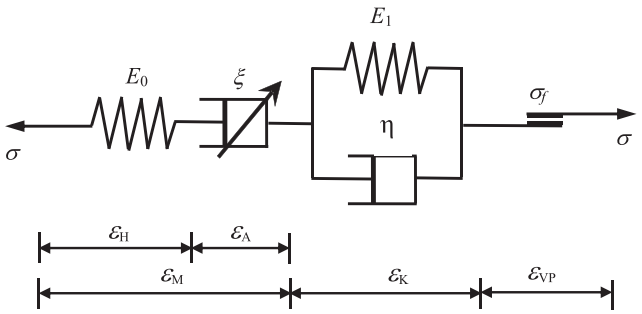


**Fig. 5** Sketch of the fractional order rheological model in one-dimensional form

## Three-dimensional creep model

To verify the correctness of the model which enables to be used in engineering analysis, the one-dimensional creep equation must be extended into a three-dimensional equation to further develop a numerical program (Chen et al. 2017; Xu and Ni 2019). Here, the nonassociated Mohr-Coulomb flow rule was adopted; when the yield function was$f < 0$, it was required to update the stress by plastic strain increments, and the three-dimensional model was established.

The elastic constitutive relationship in one dimension is $\sigma = E\varepsilon_e$, while the three-dimensional relationship in tensor form is as follows:

$$\begin{cases} S_{ij} = 2G_0 e_{ij} \\ \sigma_{ii} = 3K\varepsilon_{ii} \end{cases} \tag{25}$$

where $S_{ij}$, $e_{ij}$, $\sigma_{ii}$ and $\varepsilon_{ii}$ are the tensor forms of the stress deviator, the strain deviator, the stress first invariant and the strain first invariant, respectively.

Under three-dimensional stress conditions, the total strain fractional order creep model can be expressed as follows:

$$\varepsilon_{ij} = \varepsilon_{ij}^{M} + \varepsilon_{ij}^{K} + \varepsilon_{ij}^{vp} \tag{26}$$

The deviator strain rate can be obtained by solving Eq. 27:

$$\dot{e}_{ij} = \dot{e}_{ij}^{M} + \dot{e}_{ij}^{K} + \dot{e}_{ij}^{vp} \tag{27}$$

where $\dot{e}_{ij}$, $\dot{e}_{ij}^{M}$, $\dot{e}_{ij}^{K}$ and $\dot{e}_{ij}^{vp}$ are the total deviator strain rate, deviator strain rate of the Hooke body, deviator strain rate of the Kelvin body and deviator strain rate of the Saint-Venant body, respectively.

For a similar Maxwell body, the deviator strain rate can be written as follows:

$$\dot{e}_{ij}^{M} = \frac{\dot{S}_{ij}}{2G^{M}} + \frac{S_{ij}}{2\xi}\frac{t^{\beta-1}}{\Gamma(\beta)}, 0 \le \beta \le 1 \tag{28}$$

where $S_{ij}$ is the total deviator stress, $G^{M}$ is the bulk modulus of the Hooke body and $\xi$ is the viscous coefficient of the Abel dashpot.

For the Kelvin body, the deviator strain rate can be written as follows:

$$S_{ij} = 2\eta^{K}\dot{e}_{ij}^{K} + 2G^{K}e_{ij}^{K} \tag{29}$$

For the Saint-Venant body, the deviator strain rate can be written as follows:

$$\dot{e}_{ij}^{vp} = \lambda\frac{\partial g}{\partial \sigma_{ij}} - \frac{1}{3}\dot{e}_{\mathrm{vol}}^{vp}\delta_{ij} \tag{30}$$

$$\dot{e}_{\mathrm{vol}}^{vp} = \lambda\left[\frac{\partial g}{\partial \sigma_{11}} + \frac{\partial g}{\partial \sigma_{22}} + \frac{\partial g}{\partial \sigma_{33}}\right] \tag{31}$$

In general, the spherical stress rate does not generate plastic deformation; therefore, the spherical stress rate in the fractional rheological model can be written as follows:

$$\dot{\sigma}_m = K\left(\dot{e}_{\mathrm{vol}} - \dot{e}_{\mathrm{vol}}^{vp}\right) \tag{32}$$

Considering the damage, Eq. 32 can be rewritten as follows:

$$\dot{\sigma}_m = K\left[1 - D\left((\sigma + \Delta\sigma)/\sigma_f\right)\right]\left(\dot{e}_{\mathrm{vol}} - \dot{e}_{\mathrm{vol}}^{vp}\right) \tag{33}$$

where $\dot{\sigma}_m$ is the spherical stress rate, $\dot{e}_{\mathrm{vol}}$ is the total spherical strain rate and $\dot{e}_{\mathrm{vol}}^{vp}$ is the spherical strain rate of the plastic component.

The combined Mohr-Coulomb yield envelope contains two criteria, i.e. the shear yield and tensile yield, and the equations in terms of the principal axial stresses are as follows:

$$f = \sigma_1 - \sigma_3 N_\phi + 2c\sqrt{N_\phi} \tag{34}$$

$$f = \sigma^t - \sigma_3 \tag{35}$$

where $c$ is the cohesion, $\phi$ is the frictional angle, $\sigma^t$ is the tensile strength and $\sigma_1$ and $\sigma_3$ are the maximum principal stress and minimum principal stress, respectively. Equation 27 can be rewritten as the following incremental form:

$$\Delta e_{ij} = \Delta e_{ij}^{M} + \Delta e_{ij}^{K} + \Delta e_{ij}^{vp} \tag{36}$$

and Eq .29 can be rewritten as follows:

$$\Delta e_{ij}^{M} = \frac{\Delta S_{ij}}{2G^{M}} + \frac{\overline{S}_{ij}}{2\xi}\frac{(t+\Delta t)^{\beta} - t^{\beta}}{\Gamma(1+\beta)} \tag{37}$$

Considering $1 \le 1 + \beta \le 2$ and by substituting Eq. 17 into Eq. 37, we obtain the following:

$$\Delta e_{ij}^{M} = \frac{\Delta S_{ij}}{2G^{M}} + \frac{\overline{S}_{ij}}{2\xi}\frac{(t+\Delta t)^{\beta} - t^{\beta}}{(0.447z^2 - 1.326z + 1.869)} \tag{38}$$

Equation 29 can be rewritten as the following:

$$S_{ij}\Delta t = 2\eta^{K}\Delta e_{ij}^{K} + 2G^{K}e_{ij}{}^{K}\Delta t \tag{39}$$

where $\overline{S}_{ij}$ and $\overline{e}_{ij}{}^{K}$ are the average deviatoric stress and the average deviatoric strain of the Kelvin body in time increment steps, respectively.

$$\overline{S}_{ij} = \frac{S_{ij}^{N} + S_{ij}^{O}}{2} \tag{40}$$

$$\overline{e}_{ij} = \frac{e_{ij}^{N} + e_{ij}^{O}}{2} \tag{41}$$

where '$N$' and '$O$' are the new value and the old value in time increment steps, respectively; $S_{ij}^{N}$ and $S_{ij}^{O}$ are the new deviatoric stress and the old deviatoric stress in time increment steps, respectively; and $e_{ij}^{N}$ and $e_{ij}^{O}$ are the new deviatoric strain and the old deviatoric strain, respectively.

Combining the damage variable and its evolution equation, the equations for the instantaneous damage variable increment and time-dependent damage variable increment can be expressed as follows:

$$\Delta D(\sigma/\sigma_f) = 36.37\left[\exp\left(-7.143(\sigma+\Delta\sigma)/\sigma_f\right)-\exp\left(-7.143\sigma/\sigma_f\right)\right] \tag{42}$$

$$\Delta D(t/t_F) = [1-(t+\Delta t)/t_F]^{\gamma}-(1-t/t_F)^{\gamma} \tag{43}$$

Equations 37 and 39 can be written as follows:

$$\Delta e_{ij}^{M} = \frac{\Delta S_{ij}}{2G^{M}\left[0.64+36.37\exp\left(-7.143(\sigma+\Delta\sigma)/\sigma_f\right)\right]} + \frac{\overline{S}_{ij}}{2\xi[1-(t+\Delta t)/t_F]^{\gamma}}\frac{(t+\Delta t)^{\beta}-t^{\beta}}{(0.447z^2-1.326z+1.869)} \tag{44}$$

$$\overline{S}_{ij}\Delta t = [1-(t+\Delta t)/t_F]^{\gamma}\left(2\eta^{K}\Delta e_{ij}^{K}+2G^{K}\overline{e}_{ij}^{\,k}\Delta t\right) \tag{45}$$

Substituting Eqs. 40 and 41 into Eq. 44, we obtain the following:

$$e_{ij}^{K,N} = \frac{1}{A}\left[Be_{ij}^{K,O}+\frac{\Delta t}{4\eta^{K}[1-(t+\Delta t)/t_F]^{\gamma}}\left(S_{ij}^{N}+S_{ij}^{O}\right)\right] \tag{46}$$

$$A = 1+\frac{G^{K}\Delta t}{2\eta^{K}}, B = 1-\frac{G^{K}\Delta t}{2\eta^{K}} \tag{47}$$

Substituting Eqs. 45 and 46 into Eq. 36, we obtain the following:

$$S_{ij}^{N} = \frac{1}{a}\left[\Delta e_{ij}-\Delta e_{ij}^{vp}+bS_{ij}^{O}-\left(\frac{B}{A}-1\right)e_{ij}^{K,O}\right] \tag{48}$$

where:

$$a = \frac{1}{2G^{M}}\frac{1}{\left[0.64+36.37\exp\left(-7.143(\sigma+\Delta\sigma)/\sigma_f\right)\right]} + \frac{1}{[1-(t+\Delta t)/t_F]^{\gamma}}\left[\frac{1}{4\xi}\frac{(t+\Delta t)^{\beta}-t^{\beta}}{(0.447z^2-1.326z+1.869)}+\frac{\Delta t}{4A\eta^{K}}\right] \tag{49}$$

$$b = \frac{1}{2G^{M}}\frac{1}{\left[0.64+36.37\exp\left(-7.143(\sigma+\Delta\sigma)/\sigma_f\right)\right]} - \frac{1}{[1-(t+\Delta t)/t_F]^{\gamma}}\left[\frac{1}{4\xi}\frac{(t+\Delta t)^{\beta}-t^{\beta}}{(0.447z^2-1.326z+1.869)}+\frac{\Delta t}{4A\eta^{K}}\right] \tag{50}$$

Additionally, the spherical stress can be written as the following differential form:

$$\sigma_m^{N} = \sigma_m^{O}+K\left[1-D\left((\sigma+\Delta\sigma)/\sigma_f\right)\right]\left(\Delta e_{\mathrm{vol}}-\Delta e_{\mathrm{vol}}^{\mathrm{vp}}\right) \tag{51}$$

The new spherical strain of the Kelvin body can be obtained from Eq. 46:

$$e_o^{K,N} = \frac{1}{C}\left[De_o^{K,O}+\frac{\Delta t}{6K}\left(\sigma_o^{N}+\sigma_o^{O}\right)\right], C = 1+\frac{K\Delta t}{2\eta^{K}}, D = 1-\frac{K\Delta t}{2\eta^{K}} \tag{52}$$

The improved fractional order model can be expressed as Eqs. 48 and 51, which are convenient for compiling programs.

## Verification of the creep damage constitutive model

To verify the rationality of the fractional order creep damage model and the correctness of the numerical program, the triaxial creep experiments of the Jinping II marble were simulated by the established model. The model sizes were consistent with the laboratory-tested standard samples with a height of 100 mm and a diameter of 50 mm. The parameters for the creep simulations are listed in Table 3.

According to the laboratory creep test process, test results of 40 MPa confining pressure was simulated, and the creep time in the numerical simulation was in accordance with the actual test. Figure 6 shows the simulation creep results of the specimens under 140 MPa and 150 MPa deviatoric stresses compared with the test results.

Experimental and simulation results agreed very well, which indicated that the time-dependent creep model was reasonable and that the developed numerical program was valid.

# Long-time deformation analysis for the Jinping II underground caverns

## Numerical model and parameters

According to the above fractional order time-dependent creep constitutive model, the long-term stability of the Jinping II hydropower station was analysed based on the monitored data at 5 key positions in section K0+062 (Jiang et al. 2020c). In the numerical analysis, a 3D meshed model with more than 1.16 million elements was used.

**Table 3** Mechanical parameters for the simulating the experimental results

| Loads (MPa) | $E_0$ (GPa) | $E_1$ (GPa) | $\eta$ (GPa h) | $\xi$ (GPa h) | $\beta$ |
|---|---|---|---|---|---|
| 140 | 37.9 | 63.8 | 822 | 1070 | 0.37 |
| 150 | 15.5 | 46.3 | 525 | 576 | 0.51 |

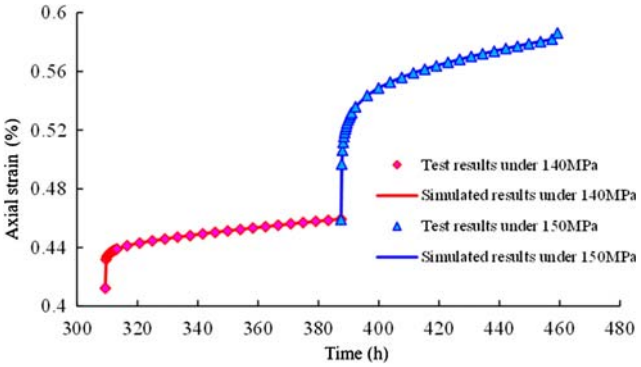


**Fig. 6** Comparison between the test results and simulated results under deviatoric stresses of 140 MPa and 150 MPa, respectively

## Long-time deformation prediction of surrounding rock

Based on displacement increment sensitivity analysis, Chen et al. (2019) proposed the intelligent back analysis method of the rock mass creep parameters for large underground caverns. This method utilized the displacements of the arch roof, arch shoulder and sidewall as characteristic indexes, with five creep parameters, i.e. the instantaneous shear modulus, viscosity coefficient, viscoelastic shear modulus, viscoelastic coefficient and fractional order value β, which were confirmed by inversion analysis. A multi-data fusion fitting function was also established to conduct inversion of the creep parameters, and the parameter values were confirmed by adopting a genetic algorithm-neural network search of the global space (as shown in Table 4).

According to these parameters determined via inversion analysis, we calculated the time-dependent deformation of the Jinping II underground caverns. Figure 7 shows the time evolution characteristics of the surrounding rock in the 2-2 section after excavation at 2 years, 10 years, 20 years and 50 years. The results demonstrated that the largest displacement of the main powerhouse occurred in the upstream sidewall, and the smallest displacement was located at the arch during the long-term deformation. The largest displacement of the main transformer chamber occurred in the downstream sidewall, while the smallest displacement was in the upstream abutment. The largest displacement of the tailrace chamber was located in the upstream sidewall, with the smallest displacement occurring in the upstream abutment. The long-time deformation prediction revealed that the surrounding rock of Jinping II hydropower station is safe in the long-term operation.

## Conclusions

The onsite investigation revealed that the time-dependent performance of surrounding rock in the underground caverns performance as an increase in rock's deformation. The in situ failure modes of the marble included shallow cracking, detachment of the surrounding rock and spalling or breakage of the shotcrete.

Laboratory creep tests for the damaged Jinping marble showed that these marble specimens with initial damage exhibited more pronounced creep behaviours under certain stress conditions: (a) Instantaneous deformation and the axial creep strain occurred very quickly after the load was applied, (b) The steady creep stage was observed when the axial load reached nearly 80% of the instant peak strength of the marble, (c) creep rate increased rapidly until the rock failed when the constant load nearly reached the triaxial strength. The corresponding CT test results indicated that creep failures of the initial damaged marble exposed diagonal fracture faces that could be attributed to shear failure.

A new time-dependent creep constitutive model was proposed to characterize the creep mechanical behaviours of the marble in terms of the fractional derivatives and damage variables by replacing the Newtonian dashpot with the Abel dashpot. Furthermore, this one-dimensional creep equation was extended to a three-dimensional numerical model to verify its reasonability and to analyse the long-term deformation tendency of the Jinping II underground caverns. The comparison of the simulation analysis results with the measured results indicated that the proposed model provided a new way to describe the full creep process of damaged marble in studying the stability of underground engineering structures with damaged surrounding rock.

**Table 4** Creep parameters of the rock mass by back analysis

| Parameters | Instantaneous shear modulus (GPa) | Viscosity coefficient (GPa h) | Viscoelastic shear modulus (GPa) | Viscoelastic coefficient (GPa h) | $\beta$ |
|---|---|---|---|---|---|
| Inversion values | 511.06 | 1.07 | 82.86 | 219.19 | 0.32 |

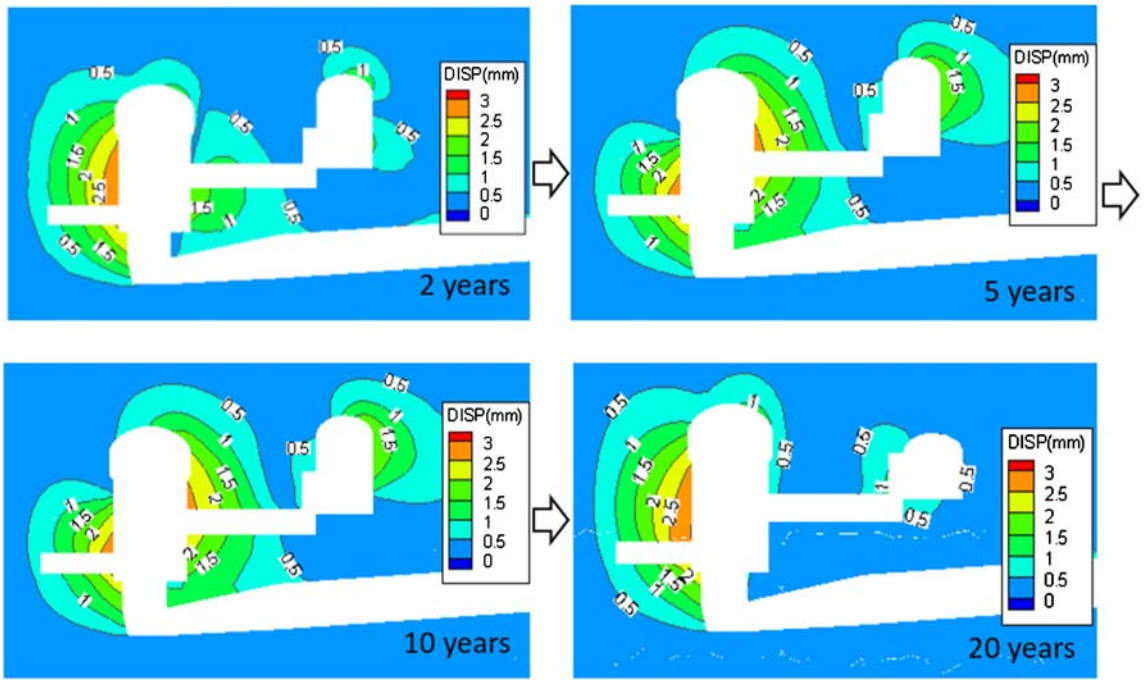


**Fig. 7** Time evolution of the caverns' spatial deformation in monitoring section 2-2 from 2 to 20 years

**Acknowledgements** The authors received the financial supports from the National Natural Science Foundation of China (Grant No. U1765206 and No. 41672314) and Anhui Province Natural Science Foundation (No. 1508085QE101).

## References

Bagley RL, Torvik PJ (1983) A theoretical basis for the application of fractional calculus to viscoelasticity. J Theol 27(3):201–210. https://doi.org/10.1122/1.549724

Bian K, Liu J, Zhang W, Zheng XQ, Ni SH, Liu ZP (2019) Mechanical behavior and damage constitutive model of rock subjected to water-weakening effect and uniaxial loading. Rock Mech Rock Eng 52(1): 97–106. https://doi.org/10.1007/s00603-018-1580-4

Brady BHG, Brown ET (1985) Rock mechanics for underground mining. Springer, Dordrecht

Cai TT, Feng ZC, Jiang YL (2018) An improved hardening-damage creep model of lean coal: a theoretical and experimental study. Arab J Geosci 11(20):645. https://doi.org/10.1007/s12517-018-4012-6

Chen J (2013) Time-dependent deformation and fracture mechanisms of hard rock and engineering behavioural analysis. Institute of Rock and Soil Mechanics, Chinese Academy of Sciences, Wuhan

Chen LW, Li SJ, Zhang KX (2017) Secondary development and application of the NP-T creep model based on FLAC3D. Arab J Geosci 10:508. https://doi.org/10.1007/s12517-017-3301-9

Chen J, Jiang Q, Feng XT, Hu YR (2019) Intelligent back analysis of rock mass creep parameters for large underground caverns under high in-situ stress based on incremental displacement. J China Coal Soc 44(5):1446–1455. https://doi.org/10.13225/j.cnki.jccs.2019.6021

Feng XT, Chen BR, Yang CX, Zhou H, Ding XL (2004) Identification of visco-elastic models for rocks using genetic programming coupled with the modified particle swarm optimization algorithm. Int J Rock Mech Min Sci 43(5):789–801. https://doi.org/10.1016/j.ijrmms.2005.12.010

Feng XT, Guo HS, Yang CX, Li SJ (2018a) In situ observation and evaluation of zonal disintegration affected by existing fractures in deep hard rock tunneling. Eng Geol 242:1–11. https://doi.org/10.1016/j.enggeo.2018.05.019

Feng XT, Yao ZB, Li SJ, Wu SY, Yang CX, Guo HS, Zhong S (2018b) In situ observation of hard surrounding rock displacement at 2400-m-deep tunnels. Rock Mech Rock Eng 51(3):873–892. https://doi.org/10.1007/s00603-017-1371-3

Herrmann J, Rybacki E, Sone H, Dresen G (2019) Deformation experiments on Bowland and Posidonia Shale-part II: creep behavior at in situ pc–T conditions. Rock Mech Rock Eng 52(2):755–779. https://doi.org/10.1007/s00603-019-01941-2

Hu B, Yang SQ, Xu P (2018) A nonlinear rheological damage model of hard rock. J Cent South Univ 25(7):1665–1677. https://doi.org/10.1007/s11771-018-3858-9

Jiang Q, Feng XT, Li SJ et al (2019) Cracking-restraint design method for large underground caverns with hard rock under high geostress condition and its practical application. Chin J Rock Mech Eng 38(6): 1081–1100. https://doi.org/10.13722/j.cnki.jrme.2018.1147

Jiang Q, Yang B, Fei Y et al (2020a) New method for characterizing the shear damage of natural rock joint based on 3D engraving and 3D scanning. Int J Geomech 20(2):06019022. https://doi.org/10.1061/(ASCE)GM.1943-5622.0001575

Jiang Q, Zhong S, Pan P et al (2020b) Observe the temporal evolution of deep tunnel's 3D deformation by 3D laser scanning in the Jinchuan No. 2 Mine. Tunn Undergr Space Technol 97:103237. https://doi.org/10.1016/j.tust.2019.103237

Jiang Q, Liu XP, Yan F et al (2020c) Failure performance of 3DP physical twin-tunnel model and corresponding safety factor evaluation. Rock Mech Rock Eng (Online). https://doi.org/10.1007/s00603-020-02244-7

Kawada Y, Yajima T, Nagahama H (2013) Fractional-order derivative and time-dependent viscoelastic behaviour of rocks and minerals.

Acta Geophys 61(6):1690–1702. https://doi.org/10.2478/s11600-013-0153-x
Koeller RC (1984) Application of fractional calculus to the theory of viscoelasticity. J Appl Mech 51(2):299–307. https://doi.org/10.1115/1.3167616
Koeller RC (2007) Toward an equation of state for solid materials with memory by use of the half-order derivative. Acta Mech 191(3-4):25–133. https://doi.org/10.1007/s00707-006-0411-y
Li SJ, Feng XT, Li ZH, Chen BR, Jiang Q, Wu SY, Hu B, Xu JS (2011) In situ experiments on width and evolution characteristics of excavation damaged zone in deeply buried tunnels. Sci China-Technol Sci 54(SI):167–174. https://doi.org/10.1007/s11431-011-4637-0
Liu N (2011) Time-dependent behaviour of crack propagation in deep marble and long-term stability assessment of tunnel. Postdoctoral Thesis
Liu X, Li D, Han C (2020) A nonlinear damage creep model for sandstone based on fractional theory. Arab J Geosci 13:246. https://doi.org/10.1007/s12517-020-5215-1
Lu B, Wang JM, Ding XL, Wu AQ, Duan SH, Huang SL (2010) Study of deformation and cracking mechanism of surrounding rock of Jinping I underground powerhouse. Chin J Rock Mech Eng 29(12):2429–2441
Lu DC, Kong FC, Du XL, Shen CP, Su CC, Wang J (2020) Fractional viscoelastic analytical solution for the ground displacement of a shallow tunnel based on a time-dependent unified displacement function. Comput Geotech 117. https://doi.org/10.1016/j.compgeo.2019.103284
Malan DF (2002) Manuel rocha medal recipient simulating the time-dependent behaviour of excavations in hard rock. Rock Mech Rock Eng 35(4):225–254. https://doi.org/10.1007/s00603-002-0026-0
Martin CD (1993) The strength of massive Lac du Bonnet granite around underground openings. Doctoral Thesis. The United States: University of Manitoba
Martino JB, Chandler NA (2004) Excavation-induced damage studies at the underground research laboratory. Int J Rock Mech Min Sci 41(8):1413–1426. https://doi.org/10.1016/j.ijrmms.2004.09.010
Millard A, Jobst M, Amel R, Uehara S (2009) Study of the initiation and propagation of excavation damaged zones around openings in argillaceous rock. Environ Geol 57(6):325–1335. https://doi.org/10.1007/s00254-008-1518-3
Paraskevopoulou C, Perras M, Diederichs M, Loew S, Lam T, Jensen M (2018) Time-dependent behaviour of brittle rocks based on static load laboratory tests. Geothch Geol Eng 36(1):337–376. https://doi.org/10.1007/s10706-017-0331-8
Pu SY, Zhu ZD, Song L, Song WL, Peng YY (2020) Fractional-order visco-elastoplastic constitutive model for rock under cyclic loading. Arab J Geosci 13:326. https://doi.org/10.1007/s12517-020-05288-9
Rabotnov YN (1963) On the equations of state for creep. In: Progress in Applied Mechanics (Prager Anniversary Volume). MacMillan, New York
Radmanesh M, Ebadi MJ (2020) A local mesh-less collocation method for solving a class of time-dependent fractional integral equations: 2D fractional evolution equation. Eng Anal Bound Elem 113:372–381. https://doi.org/10.1016/j.enganabound.2020.01.017
Rassouli FS, Zoback MD (2017) A comparison of short-term and long-term creep experiments in unconventional reservoir formations. 50th US Rock Mechanics/Geomechanics Symposium. 26-29 June, Houston, Texas
Rogers L (1983) Operators and fractional derivatives for viscoelastic constitutive equations. J Rheol 27:351–372. https://doi.org/10.1122/1.549710
Scheidegger AE (1970) Stochastic models in hydrology. Water Resour Res 6(3):750–755. https://doi.org/10.1029/wr006i003p00750
Sharifzadeh M, Sharifi M, Delbari SM (2010) Back analysis of an excavated slope failure in highly fractured rock mass: the case study of Kargar slope failure (Iran). Environ Earth Sci 60(1):183–192. https://doi.org/10.1007/s12665-009-0178-2
Shi GC, Yang XJ, Yu HC, Zhu C (2019) Acoustic emission characteristics of creep fracture evolution in double-fracture fine sandstone under uniaxial compression. Eng Fract Mech 210(s1):13–28. https://doi.org/10.1016/j.engfracmech.2018.09.004
Vakili A (2016) An improved unified constitutive model for rock material and guidelines for its application in numerical modelling. Comput Geotech 80:261–282. https://doi.org/10.1016/j.compgeo.2016.08.020
Wang YS, Ma LJ, Wang MY (2018) A creep constitutive model incorporating deformation mechanisms for crushable calcareous sand. Arab J Geosci 11:623. https://doi.org/10.1007/s12517-018-3982-8
Wang JB, Zhang Q, Song ZP, Zhang YW (2020) Creep properties and damage constitutive model of salt rock under uniaxial compression. Int J Damage Mech 29(6):902–922. https://doi.org/10.1177/1056789519891768
Weng MC (2014) A generalized plasticity-based model for sandstone considering time-dependent behavior and wetting deterioration. Rock Mech Rock Eng 47:1197–1209. https://doi.org/10.1007/s00603-013-0466-8
Wu F, Liu JF, Wang J (2015) An improved Maxwell creep model for rock based on variable-order fractional derivatives. Environ Earth Sci 73(11):6965–6971. https://doi.org/10.1007/s12665-015-4137-9
Xu HY, Jiang XY (2017) Creep constitutive models for viscoelastic materials based on fractional derivatives. Comput Math Appl 73(6):1377–1384. https://doi.org/10.1016/j.camwa.2016.05.002
Xu JC, Ni YD (2019) Displacement ratio dichotomy back analysis of surrounding rock-initial support system of weathered rock tunnel. Arab J Geosci 12(6):181. https://doi.org/10.1007/s12517-019-4334-z
Xu WY, Wang RB, Wang W, Zhang ZL, Zhang JC, Wang WY (2012) Creep properties and permeability evolution in triaxial rheological tests of hard rock in dam foundation. J Cent South Univ 19(1):252–261. https://doi.org/10.1007/s11771-012-0999-0
Yang SQ, Xu P, Xu T (2015) Nonlinear visco-elastic and accelerating creep model for coal under conventional triaxial compression. Geomech Geophys Geo-Energy Geo-Resour 1(3-4):109–120. https://doi.org/10.1007/s40948-015-0014-y
Yang XJ, Wang JM, Zhu C, He MC (2019) Effect of water on long-term strength of column rocks based on creep behavior in Yungang Grottoes. China Geotech Geol Eng 37(1):173–183. https://doi.org/10.1007/s10706-018-0601-0
Zhang ZP, Zhang R, Xie HP, Liu J, Were P (2015) Differences in the acoustic emission characteristics of rock salt compared with granite and marble during the damage evolution process. Environ Earth Sci 73(11):6987–6999. https://doi.org/10.1007/s12665-015-4406-7
Zhao J, Feng XT, Zhang XW, Yang CX (2019) Brittle and ductile creep behavior of Jinping marble under true triaxial stress. Eng Geol 258:105157. https://doi.org/10.1016/j.enggeo.2019.105157
Zhou HW, Wang CP, Han BB, Duan ZQ (2011) A creep constitutive model for salt rock based on fractional derivatives. Int J Rock Mech Min Sci 48(1):116–121. https://doi.org/10.1016/j.ijrmms.2010.11.004
Zhou HW, Yi HY, Mishnaevsky L Jr, Wang R, Duan ZQ, Chen Q (2016) Deformation analysis of polymers composites: rheological model involving time-based fractional derivative. Mech Time-Depend Mater 21(2):151–161. https://doi.org/10.1007/s11043-016-9323-y